Center for Turbulence Research
Proceedings of the Summer Program 2008

Thermocapillary motion of deformable drops and bubbles

By M. Herrmann, J. M. Lopez, P. Brady AND M. Raessi

In this paper we report on a numerical method to include Marangoni forces into a finite-volume solver for multi-phase flows. Our work is motivated by the question of whether thermal fluctuations typically found in combustion applications can impact the atomization of fuel drops due to variations in surface tension. To verify and validate our proposed method, we compare our results to theoretically predicted thermocapillary migration velocities of drops and to experimentally measured migration velocities in micro-gravity environments.

1. Introduction

Thermal fluctuations can have a significant impact on the dynamics of liquid/gas interfaces because, for most gas/liquid combinations, both surface tension and phase transition depend strongly on the local temperature. An important technical application where both surface tension forces and phase transition are dominant is the atomization of liquid fuels for combustion processes. For combustion to occur, the liquid fuel needs to be atomized, evaporated, and mixed with an oxidizer. The ensuing chemical reactions can generate temperature variations on the order of 10^3K over small length scales of the order of 10^{-3}m. Since all processes typically occur in a turbulent environment, the phase interface itself is subjected to a broad range of local temperature fluctuations. Due to the strong dependence of surface tension on temperature, the temperature fluctuations result in Marangoni forces that impact the flowfield at the gas/liquid interface, which in turn alter the interfacial temperature distribution via the induced interfacial flow (Levich & Krylov 1969). Although the ratio of global inertial to surface tension forces is typically large in these applications, atomization, which is the first in the sequence of processes leading to combustion, always occurs on small scales (involving droplets which are many orders of magnitude smaller than the diameter of the initial liquid jet). At these scales, surface tension forces are dominant. Variations in temperature, resulting in variations in surface tension forces, can thus influence atomization significantly.

Another example where the temperature-dependent surface tension influences the dynamics of phase interfaces is the thermocapillary motion of drops and bubbles. The study of the thermocapillary motion was first reported by Young, Goldstein & Block (1959), who determined the terminal velocity of a spherical drop in the creeping flow limit. Under those conditions, the drop does not deform and a steady migration is achieved in an environment with a linear temperature profile. There have been numerous subsequent studies relaxing the creeping flow limit, but for the most part these have neglected any deformations of the drop (see the reviews Subramanian 1992; Subramanian, Balasubramaniam & Wozniak 2002). The main motivation for those studies stems from microgravity applications in which the velocities involved may be small enough to justify neglecting

deformations, but for our interests in non-isothermal effects in atomization, deformations are important. It appears that the first numerical study of surface deformations due to thermocapillary motion of a bubble is Chen & Lee (1992). Their axisymmetric computations showed that deformations tend to reduce the bubble's velocity. The first 3-D computations of the thermocapillary motion of deforming drops or bubbles were presented by Haj-Hariri, Shi & Borhan (1997). For the parameter regimes they considered, they found that the drops or bubbles remain axisymmetric, but deform into either oblate or prolate spheroids depending on the density ratio between the drop/bubble and the bulk, as predicted earlier in the axisymmetric analysis in the limit of large thermal diffusivity by Balasubramaniam & Chai (1987). In an axisymmetric numerical study of a deforming bubble with larger inertia, Welch (1998) found that not only does the velocity of the bubble reduce with deformation, but that for large enough inertia the bubble does not settle to a steady velocity.

Nas & Tryggvason (2003) and Nas, Muradoglu & Tryggvason (2006) considered the interaction between a number of deformable 3-D drops in a temperature gradient. In those studies, they also considered the single drop case in the creeping flow limit (as a test problem for their numerics), but only considered non-zero inertia for the multiple bubble simulations, for which they found strong interactions in contrast to the case of multiple bubbles in the creeping flow limit where there is no interaction (Acrivos *et al.* 1990). It thus appears that the only 3-D deformable drop studies with non-zero inertia for a single drop are those of Haj-Hariri *et al.* (1997). Very recently diffuse-interface models using a phase-field approach have been reported (Borcia & Bestehorn 2007) that account for a temperature-dependent generalized surface tension (in the phase-field sense), but the numerical results have so far been restricted to 2-D flows.

Experimental investigations of the thermocapillary motion of drops and bubbles are hampered by gravitational effects which tend to mask the thermocapillary effect, unless they are conducted in a low-gravity environment. A number of experiments have been conducted in drop towers, sounding rockets and aboard space shuttles; see the extensive review of Subramanian, Balasubramaniam & Wozniak (2002). Some of the more recent experiments motivate our present investigation. These experiments have noted complicated transients and time-dependent behavior in regimes where the flow has finite viscous and thermal inertia (Treuner *et al.* 1996; Hadland *et al.* 1999; Wozniak *et al.* 2001). Those experimental studies noted that there are no theoretical or numerical results with which to compare their experiments. For a viscous drop there are four time scales which come into play in determining the transient evolution: r_0^2/ν_d, r_0^2/ν_b, r_0^2/α_d, r_0^2/α_d, where r_0 is the drop radius, ν is the kinematic viscosity, α is the thermal diffusivity, and the subscripts d and b refer to the drop and bulk liquids, respectively. In the microgravity experiments these time scales differ by up to two orders of magnitude within a single experimental run, and so complicated temporal behavior is not surprising. The experiments in the drop tower (Treuner *et al.* 1996), having the relative luxury of being able to repeat many experimental runs under nominally the same conditions, noted that the problem is very sensitive to initial conditions. It has also been noted by several investigators that in the experiments it has not been possible to determine the initial temperature distribution inside the drop. A recent numerical study with non-deforming spherical bubbles noted that the early transients are very sensitive to the initial temperature distribution (Yin *et al.* 2008). Furthermore, the liquids used in the experiments (silicon oils for the bulk phase) have temperature-dependent viscosity and density, and for the temperature gradients used these variations are non-trivial. All of the presently

available theoretical or numerical results assume constant fluid properties, except for the surface tension which is assumed to vary linearly with temperature. The review article Subramanian, Balasubramaniam & Wozniak (2002) concluded that the most important theoretical problem that needs to be addressed for an isolated drop is the consideration of the fully transient problem accommodating the dependence of physical properties on temperature.

In this paper a numerical method for finite-volume flow solvers to consistently incorporate the Marangoni forces is verified and validated using both theoretical and experimental data.

2. Governing equations and numerical technique

Consider the fate of a spherical drop of one fluid with radius r_0 placed in an initially quiescent bulk fluid with an imposed (typically positive) linear temperature gradient G_T in the vertical direction. The two fluids are immiscible with, in general, different densities, viscosities and thermal properties. We shall assume that the surface tension σ^* between the two fluids varies linearly with gradient σ_T (which for most fluids of interest is negative)

$$\sigma^*(T^*) = \sigma_0 + \sigma_T(T^* - T_0^*)\,, \tag{2.1}$$

where σ_0 is the surface tension at some suitable reference temperature T_0^*.

We shall use the initial radius of the drop, r_0, as the length scale and $G_T r_0$ as the temperature scale. For the thermocapillary motion of drops and bubbles, it is customary to use $U = \sigma_T G_T r_0/\mu_b$ as the velocity scale, where μ_b is the dynamic viscosity of the bulk phase. This then gives $\mu_b/\sigma_T G_T$ as the time scale. The surface tension is scaled by σ_0, which for the problems considered here is the surface tension at the initial temperature at the center of the drop. Throughout, subscript d refers to properties of the drop phase and subscript b to those of the bulk phase.

With these scalings, the non-dimensional linear equation of state becomes

$$\sigma(T) = 1 + Ca(T - T_0)\,, \tag{2.2}$$

where T_0 is the non-dimensional initial temperature at the center of the drop, and the capillary number, which gives the relative importance of the tangential to normal stresses at the drop interface, is

$$Ca = \frac{\mu_b U}{\sigma_0} = \frac{\sigma_T G_T r_0}{\sigma_0}\,. \tag{2.3}$$

The non-dimensional Navier–Stokes equations governing the motion of an unsteady, incompressible, immiscible, two-fluid system, are

$$\rho_r\left(\frac{\partial \boldsymbol{u}}{\partial t} + \boldsymbol{u}\cdot\nabla\boldsymbol{u}\right) = -\nabla P + \frac{1}{Re}\nabla\cdot\mu_r\left(\nabla\boldsymbol{u} + \nabla^T\boldsymbol{u}\right) + \frac{1}{We}\boldsymbol{F} - \frac{\rho_r}{Fr}\hat{\boldsymbol{z}}\,, \quad \nabla\cdot\boldsymbol{u} = 0\,, \tag{2.4}$$

where $\boldsymbol{u}$ is the non-dimensional velocity, P the non-dimensional pressure, the relative dynamic viscosity $\mu_r = 1$ in the bulk phase and $\mu_r = \mu_d/\mu_b$ in the drop phase, and the relative density $\rho_r = 1$ in the bulk phase and $\rho_r = \rho_d/\rho_b$ in the drop phase. The Reynolds number is

$$Re = \frac{U r_0}{\nu_b} = \frac{\sigma_T G_T r_0^2}{\mu_b \nu_b}\,, \tag{2.5}$$

where ν_b is the kinematic viscosity of the bulk phase and is related to the dynamic

viscosity by $\mu_b = \rho_b \nu_b$. The Weber number is

$$We = Re\,Ca = \frac{\rho_b r_0 U^2}{\sigma_0}\,. \tag{2.6}$$

The Froude number is

$$Fr = U^2/g r_0 = \frac{(\sigma_T G_T r_0)^2}{\mu_b^2 g r_0}\,, \tag{2.7}$$

where g is the gravitational acceleration and $\hat{\boldsymbol{z}}$ is a unit vector in the z direction. In this paper, we consider the limit of zero gravity, for which $Fr \to \infty$.

The (dimensional) surface force $\boldsymbol{F}^*$, which is non-zero only at the location of the drop interface $\boldsymbol{x}_f$, is (Landau & Lifshitz 1959)

$$\boldsymbol{F}^*(\boldsymbol{x}) = \sigma^*(T^*)\kappa^*\delta^*\boldsymbol{n} + \nabla_{||}\sigma^*(T^*)\delta^*\,, \tag{2.8}$$

where $\boldsymbol{n}$ is the local drop interface normal and δ^* the interface delta function. Non-dimensionalizing with the above scalings, and substituting the linear equation of state for the surface tension, the non-dimensional surface force is

$$\frac{1}{We}\boldsymbol{F}(\boldsymbol{x}) = \frac{1}{Re}\left(\frac{1}{Ca}\kappa\delta\boldsymbol{n} + (T - T_0)\kappa\delta\boldsymbol{n} + \nabla_{||}T\delta\right)\,, \tag{2.9}$$

where κ the local interface curvature, and $\nabla_{||}$ the tangential surface derivative. The first two terms on the right-hand side (r.h.s) correspond to the isothermal normal stress balance and the temperature-dependent normal stress balance, and the third term corresponds to the Marangoni force. The non-dimensional Navier–Stokes equations are then

$$\begin{aligned}\rho_r\left(\frac{\partial \boldsymbol{u}}{\partial t} + \boldsymbol{u}\cdot\nabla\boldsymbol{u}\right) = &-\nabla P + \frac{1}{Re}\nabla\cdot\mu_r\left(\nabla\boldsymbol{u} + \nabla^T\boldsymbol{u}\right) \\ &+ \frac{1}{Re}\left(\frac{1}{Ca}\kappa\delta\boldsymbol{n} + (T - T_0)\kappa\delta\boldsymbol{n} + \nabla_{||}T\delta\right)\,,\end{aligned} \tag{2.10}$$

augmented by the divergence-free constraint on the velocity field imposed by the continuity equation

$$\nabla\cdot\boldsymbol{u} = 0\,. \tag{2.11}$$

The non-dimensional heat equation for the temperature is

$$\rho_r c_{p_r}\left(\frac{\partial T}{\partial t} + \nabla\cdot(T\boldsymbol{u})\right) = \frac{1}{Ma}\nabla\cdot(k_r\nabla T)\,, \tag{2.12}$$

where the relative thermal conductivity $k_r = 1$ in the bulk phase and $k_r = k_d/k_b$ in the drop, the relative specific heat $c_{p_r} = 1$ in the bulk phase and $c_{p_r} = c_{p_d}/c_{p_b}$ in the drop, and the Marangoni number is

$$Ma = \frac{U r_0 \rho_b c_{p_b}}{k_b} = \frac{U r_0}{\alpha_b} = \frac{\sigma_T G_T r_0^2}{\mu_b \alpha_b} = RePr\,, \tag{2.13}$$

where the Prandtl number

$$Pr = \nu_b/\alpha_b\,, \tag{2.14}$$

is the ratio of viscous to thermal diffusivity in the bulk phase. Note that the Marangoni number is equivalent to the Péclet number, Pe, for the characteristic velocity that is used in thermocapillary migration of drops or bubbles.

We see that this simple problem of a single drop in a temperature gradient field is

governed by several parameters. There are three parameters describing the dynamics: Re, Ca, and Ma (the other three, We, Pe, and Pr are dependent on these), three ratios of the material properties in the two phases: ρ_r, α_r, and μ_r, as well as a geometric parameter L giving the ratio of the length scale of the environment to the initial radius of the drop.

2.1. *Numerics*

To determine the location $\boldsymbol{x}_f$ of the phase interface we employ a level set approach by defining the level set scalar at the interface

$$G(\boldsymbol{x}_f, t) = 0\,, \tag{2.15}$$

with $G(\boldsymbol{x}, t) > 0$ in the drop and $G(\boldsymbol{x}, t) < 0$ in the bulk phase. Differentiating Eq. (2.15) with respect to time yields the level set equation,

$$\frac{\partial G}{\partial t} + \boldsymbol{u} \cdot \nabla G = 0\,. \tag{2.16}$$

The interface curvature κ can be expressed in terms of the level set scalar as

$$\kappa = \nabla \cdot \frac{\nabla G}{|\nabla G|}\,. \tag{2.17}$$

We solve and evaluate all level set related equations following the refined level set grid method in a separate level set solver LIT (Herrmann 2008) using an auxiliary high-resolution G-grid with the fifth-order WENO scheme of Jiang & Peng (2000) in conjunction with the third-order TVD Runge-Kutta time discretization of Shu (1988). The phase interface curvature κ is evaluated on the G-grid using a second-order-accurate interface projection method (Herrmann 2008).

The balanced force algorithm for finite-volume solvers described in detail in Herrmann (2008) is used to solve Eqs. (2.10) and (2.11). The algorithm has been implemented in the flow solver NGA (Desjardins *et al.* 2008*a*). The location of the phase interface essentially impacts three different terms in these equations directly. The first two, ρ_r and μ_r, can be calculated for finite volume solvers by

$$\rho_r = \rho_d/\rho_b \psi_{cv} + (1 - \psi_{cv})\,, \tag{2.18}$$

$$\mu_r = \mu_d/\mu_b \psi_{cv} + (1 - \psi_{cv})\,, \tag{2.19}$$

where ψ_{cv} is the drop phase volume fraction of a control volume,

$$\psi_{cv} = 1/V_{cv} \int_{V_{cv}} H(G) dV\,, \tag{2.20}$$

with V_{cv} the volume of the control volume cv. Equation (2.20) is evaluated on the fine G-grid using an algebraic expression due to van der Pijl, Segal & Vuik (2005).

The third term is the surface force, Eq. (2.9), which in the staggered grid layout used here needs to be evaluated at the cell faces. Its normal component is calculated following the Continuum Surface Force (CSF) model (Brackbill, Kothe & Zemach 1992) approximating $\delta\boldsymbol{n}$ by $\delta\boldsymbol{n} = \nabla\psi_{cv}$. The tangential derivative of the temperature is calculated by

$$\nabla_{||} T = \nabla T - (\nabla T \cdot \boldsymbol{n})\boldsymbol{n}\,, \tag{2.21}$$

where the phase interface normal vector $\boldsymbol{n}$ is evaluated on the flow solver grid by

$$\boldsymbol{n} = \frac{\nabla\psi_{cv}}{|\nabla\psi_{cv}|}\,. \tag{2.22}$$

This results in the surface force calculated by

$$\frac{1}{We}\boldsymbol{F}(\boldsymbol{x}) = \frac{1}{Re}\left(\frac{1}{Ca}\kappa\nabla\psi + (T-T_0)\kappa\nabla\psi + \nabla T|\nabla\psi| - \frac{\nabla T\cdot\nabla\psi}{|\nabla\psi|}\nabla\psi\right), \tag{2.23}$$

with all terms being evaluated at the cell faces due to the staggered grid layout.

The level set solver LIT and the flow solver NGA are coupled using the code coupling paradigm CHIMPS (Alonso *et al.* 2006).

2.1.1. *Time-step restrictions*

In addition to satisfying the convective and viscous time step (δt) restrictions, for numerical stability, δt must also satisfy a surface force time-step restriction. For the normal component of $\boldsymbol{F}^*$ this time-step restriction is (Brackbill *et al.* 1992)

$$\delta t \leq \sqrt{\frac{(\rho_b+\rho_d)(\delta x)^3}{4\pi\sigma}}, \tag{2.24}$$

where δx is the flow solver mesh size. To derive a time-step restriction due to the tangential component of $\boldsymbol{F}^*$, we perform an analysis similar to the one given by Kang *et al.* (2000):

We denote the tangential component of $\boldsymbol{F}^*$ as

$$\boldsymbol{F}^t = F_i^t\hat{\boldsymbol{e}}_i = \nabla_{||}\sigma^*\delta^*. \tag{2.25}$$

Including $\boldsymbol{F}^t$ in the convection estimate, we approximate the bound on the i-component of $\boldsymbol{u}$ at the end of a time-step as

$$|u_i|_{\max} + \delta t|F_i^t|_{\max}/\rho_{\min}. \tag{2.26}$$

Considering the grid size in the i-direction, δx_i, we then have

$$\left(|u_i|_{\max} + \delta t|F_i^t|_{\max}/\rho_{\min}\right)\delta t/\delta x_i \leq 1, \tag{2.27}$$

which yields

$$\delta t \leq \frac{-|u_i|_{\max} + \sqrt{|u_i|_{\max}^2 + 4|F_i^t|_{\max}\delta x_i/\rho_{\min}}}{2|F_i^t|_{\max}/\rho_{\min}}, \tag{2.28}$$

or

$$\delta t \leq \frac{-|u_i|_{\max}/\delta x_i + \sqrt{(|u_i|_{\max}/\delta x_i)^2 + 4|F_i^t|_{\max}/(\rho_{\min}\delta x_i)}}{2|F_i^t|_{\max}/(\rho_{\min}\delta x_i)}, \tag{2.29}$$

Multiplying and dividing the r.h.s. of Eq. (2.29) by $|u_i|_{\max}/\delta x_i + \sqrt{(|u_i|_{\max}/\delta x_i)^2 + 4|F_i^t|_{\max}/(\rho_{\min}\delta x_i)}$ yields

$$\frac{\delta t}{2}\left(\frac{|u_i|_{\max}}{\delta x_i} + \sqrt{\left(\frac{|u_i|_{\max}}{\delta x_i}\right)^2 + \frac{4|F_i^t|_{\max}}{\rho_{\min}\delta x_i}}\right) \leq 1. \tag{2.30}$$

Since $\delta^*_{\max} = |\nabla\psi|_{\max} = 1/\delta x_{\min}$, we have $|F_i^t|_{\max} = |(\nabla_{||}\sigma^*)_i|_{\max}/\delta x_{\min}$, which gives

$$\delta t \leq 2\left[\frac{|u_i|_{\max}}{\delta x_i} + \sqrt{\left(\frac{|u_i|_{\max}}{\delta x_i}\right)^2 + \frac{4|(\nabla_{||}\sigma^*)_i|_{\max}}{\rho_{\min}\delta x_i\delta x_{\min}}}\right]^{-1}. \tag{2.31}$$

Finally, assuming a uniform grid ($\delta x_i = \delta x_{\min} = \delta x$), the time-step restriction due to the

tangential component of the surface force simplifies to

$$\delta t \leq \frac{2\delta x}{|u_i|_{\max} + \sqrt{|u_i|^2_{\max} + 4|(\nabla_{||}\sigma^*)_i|_{\max}/\rho_{\min}}}\,. \tag{2.32}$$

3. Results

In the following sections, verification and validation results for the surface force term, Eq. (2.23), implemented in the context of the finite-volume, balanced force approach are presented. In the first verification test, the thermocapillary motion of a drop in the limit of zero Marangoni will be compared to the creeping flow analytical solution of Young *et al.* (1959). In the second test, the thermocapillary motion of a planar drop between a hot and a cold plate will be analyzed and compared to experimental data for varying non-zero Marangoni numbers.

3.1. *Thermocapillary migration of a drop in the limit of zero Marangoni number*

The first test consists of a planar 2-D circular drop of diameter D of one fluid initially at rest in another fluid, both fluids having the same thermal diffusivity. The flow field is subjected to a time-invariant linear temperature profile, i.e., thermal conductivity is infinite and hence the Marangoni number is $Ma = 0$. The purpose of this test is to study the stability and accuracy of the proposed finite-volume, balanced force implementation of the Marangoni stress. In the limit of zero Marangoni number and small Reynolds number, Young *et al.* (1959) calculated the steady state velocity of a neutrally buoyant drop (sphere) in a constant temperature gradient field for two fluids of equal thermal conductivity to be

$$v_{\mathrm{YGB}} = -\frac{\sigma_T G_T D}{6\mu_b + 9\mu_d}\,. \tag{3.1}$$

The drop of diameter $D = 1$ is placed inside a 2-D box of size $5D \times 7.5D$, with the drop's center at the box centerline and $1.5D$ above the bottom wall. No-slip boundary conditions are imposed on the top and bottom wall, and periodic boundary conditions are used in the horizontal direction. A linear temperature field is imposed in the vertical direction, with $T = 0$ on the bottom wall and $T = 1$ on the top wall, resulting in $G_T = 0.1\overline{3}$. The fluid properties are $\rho_d = \rho_b = 0.2$, $\mu_b = \mu_d = 0.1$, $T_0 = 0$, $\sigma_0 = 0.1$, and $\sigma_T = -0.1$. Using these values, the theoretical rise velocity of a spherical drop is $v_{\mathrm{YGB}} = 8.88\overline{8} \times 10^{-3}$. In the simulations, the rise velocity v_r is calculated from

$$v_r = \frac{\int_V \psi v dV}{\int_V \psi dV} = \frac{\sum_{cv} \psi_{cv} v}{\sum_{cv} \psi_{cv}}, \tag{3.2}$$

where v is the vertical component of the velocity vector evaluated at the control volume centroid.

Figure 1 shows the temporal evolution of the numerically calculated rise velocity normalized by v_{YGB} for three different interface tracking methods. The left panel shows results obtained using the conservative level set/ghost fluid method of Desjardins *et al.* (2008*b*), where the Marangoni force term has been implemented according to Eq. (2.23). The center panel corresponds to a volume of fluid method used to track the phase interface (Raessi *et al.* 2007, 2008), and the right panel shows results using the RLSG method with equal resolution flow solver and G-grids are depicted. Each panel includes results using three different grid resolutions corresponding to $n_x = 64$, 128 and 256 nodes per box width. Of the three schemes, the RLSG method has the least amount of oscillations

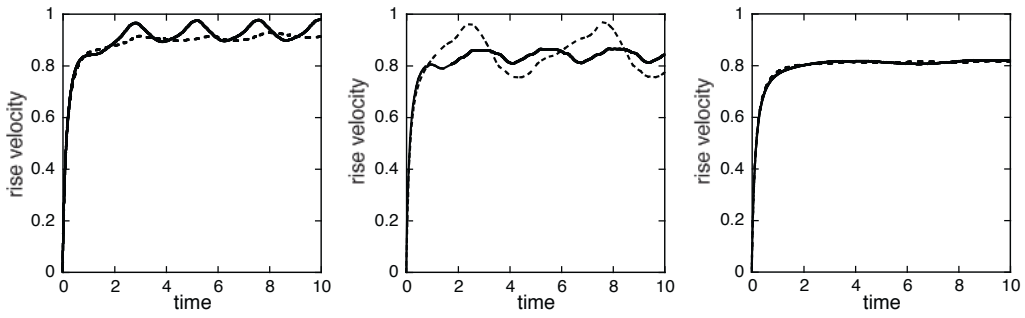

FIGURE 1. Normalized rise velocity of a planar 2-D drop in the limit of vanishing Reynolds and Marangoni numbers: conservative level set method (left), volume of fluid method (center), refined level set grid method (right). Grid sizes are $n_x = 64$ (dashed line), $n_x = 128$ (dotted line), $n_x = 256$ (solid line).

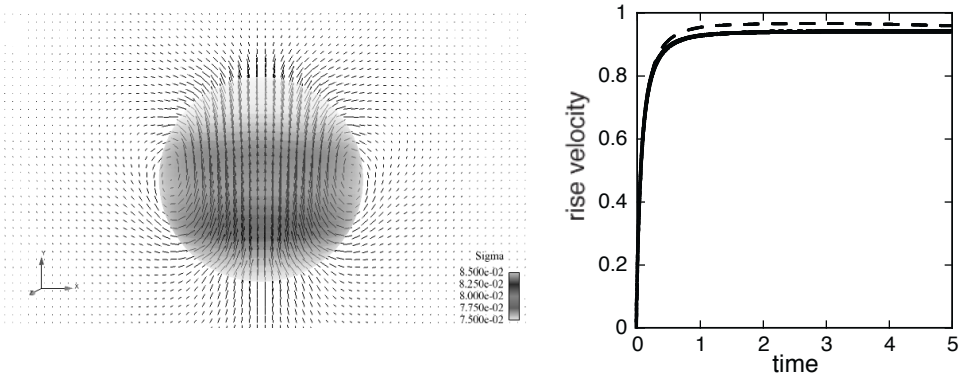

FIGURE 2. Distribution of surface force and velocity vectors in center plane (left) and normalized rise velocity in the limit of vanishing Reynolds and Marangoni numbers: 3-D case. Grid sizes are $n_x = 64$ (dashed line), $n_x = 128$ (dotted line), $n_x = 256$ (solid line).

in the rise velocity. Both VoF and RLSG methods exhibit decreasing oscillation amplitudes with increasing grid resolutions, whereas for the conservative level set/ghost fluid method the oscillation amplitude increases with increasing grid resolution. This is clearly not desirable since the asymptotic solution is a constant rise velocity. Both the VoF and RLSG methods seem to converge to a value of $v_r/v_{\mathrm{YGB}} = 0.81$, roughly 20% different from the theoretical prediction. The reason for this discrepancy is two-fold. For one, and most importantly, the theoretical rise velocity is for an axisymmetric sphere, whereas the simulations have been carried out for a planar 2-D drop. The second reason is that the simulations include small blockage effects from the finite computational domain size as well as minute deformations of the drop, whereas the theoretical formula assumes an infinite domain and a non-deformable drop.

Figure 2 shows the normalized rise velocity for a sphere, calculated using the fully 3-D RLSG method. Again grid convergence is observed, with the asymptotic value being $v_r/v_{\mathrm{YGB}} \approx 0.94$, comparable to the value of 0.97 obtained by Muradoglu & Tryggvason (2008) for the axisymmetric case. The difference in rise velocity between a planar 2-D drop and a spherical drop (0.81 compared to 0.94) is significant.

In summary, the proposed method to include the Marangoni force into a balanced force

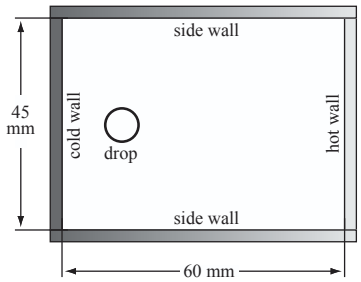

FIGURE 3. Schematic of test cell (Hadland *et al.* 1999; Wozniak *et al.* 2001).

finite-volume fluid solver using the RLSG front tracking approach yields stable results, comparable in accuracy to previously reported numerical results for axisymmetric flows.

3.2. *Thermocapillary migration of a drop with finite Marangoni number*

The second test consists of calculating the thermocapillary motion of a planar 2-D drop, using fluids of finite Marangoni numbers. Due to the finite Marangoni numbers, there is a two-way coupling between the temperature equation and the Navier-Stokes equations. This is expected to result in a reduction of the tangential temperature gradients at the drop interface due to the interfacial flow driven by the Marangoni stress, which in turn will also be reduced. Here, we aim to reproduce the experimental conditions reported in Hadland *et al.* (1999) and Wozniak *et al.* (2001).

Figure 3 shows a schematic of the test cell. It consists of a $60\,\text{mm} \times 45\,\text{mm}$ rectangular box of no-slip walls. The bottom cold wall is held at a constant $T_0 = 283\,\text{K}$, the top hot wall is held at a constant $T_1 = 343\,\text{K}$, and the side walls are held at a time invariant linear temperature profile from T_0 at the bottom to T_1 at the top. At time $t = 0\,\text{s}$, a circular drop of diameter $D = 10.7\,\text{mm}$ of Fluorinert FC-75 is released inside a bulk liquid of silicone oil (DOW-Corning DC-200 series of nominal viscosity 10 cSt). The drop's initial center is 15 mm from the bottom. At $t = 0\,\text{s}$ a linear temperature distribution from T_0 at the bottom to T_1 at the top is imposed for the bulk liquid, consistent with the experimental setup. However, in the experiments the initial temperature distribution in the drop was not measured. We therefore use an idealized initial condition where the drop has the same initial linear temperature distribution as the bulk liquid.

For the surface tension between silicone oil (DOW-Corning DC-200 series of nominal viscosity 10 cSt) and Fluorinert FC-75, we use $\sigma_0 = 0.007$ N/m and $\sigma_T = -3.6 \times 10^{-5}$ N/m K (Wozniak *et al.* 2001; Someya & Munakata 2005). The density variation with temperature of the two liquids are assumed to be of the form

$$\rho = A + BT, \tag{3.3}$$

where for the silicon oil $A = 1,200\ \text{kg/m}^3$ and $B = -0.9\ \text{kg/K m}^3$ and for the Fluorinert $A = 2,504\ \text{kg/m}^3$ and $B = -2.48\ \text{kg/K m}^3$, and the viscosity variation with temperature of the two liquids is assumed to be of the form

$$\mu = \exp(C + D/T), \tag{3.4}$$

where for the silicon oil $C = -10.17$ and $D = 1,643$ and for the Fluorinert $C = -11.76$ and $D = 1,540$ (Hadland *et al.* 1999; Wozniak *et al.* 2001). The thermal conductivity and the heat capacity of the silicone oil are set to a constant $k = 0.13389\,\text{W/mK}$ and $c_p = 1778.2\,\text{J/kgK}$, and that of the Fluorinert are $k = 0.063\,\text{W/mK}$ and $c_p = 1047.0\,\text{J/kgK}$.

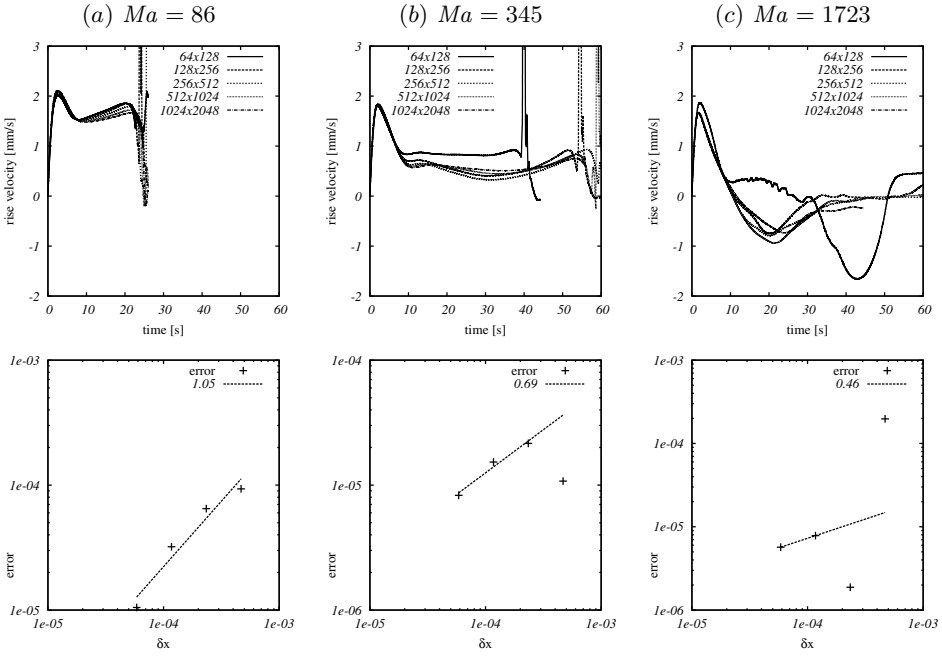

FIGURE 4. Rise velocity as function of employed grid resolution for $Re = 17.79$ and Ma as indicated.

Using the above values and relations with a reference temperature of $T = 313\,\mathrm{K}$ (evaluated at the test cell center), the reference values of the analyzed case are $Re = 17.79$, $Ma = 1723$, and $Pr = 96.86$. Note that the relatively high Marangoni number results in very thin thermal boundary layers (they scale as $Ma^{-0.5}$) that are challenging to resolve. For that reason, we consider three thermal conductivities in order to increase the thermal boundary layer thickness, corresponding to $Ma = 86, 345$ and the experimental value of $Ma = 1723$.

Figure 4 shows the rise velocity of the drop as a function of time for the three cases. All cases show an initial overshoot in the rise velocity. This is due to the imposed initial temperature gradient at the drop interface. This initial transient behavior has been observed in other transient numerical simulations (e.g., Yin *et al.* 2008). Unfortunately, available experimental data is limited to the post-initial transient regime, so the observed behavior is difficult to validate. Furthermore, there is considerable uncertainty about the exact experimental initial temperature distribution in the drop prior. If the drop is held by the injector for an extended period of time to let the drop's temperature adjust to the bulk temperature distribution, Marangoni forces will induce significant flow both in the drop and the bulk, violating the assumed initial condition of both fluids being at rest. If the drop is quickly released, the temperature distribution inside the drop does not have sufficient time to adjust, leaving the exact initial temperature distribution inside the drop unknown. In addition, the injector itself is not small compared to the drop radius and its removal from the drop may induce deformations of the initial drop shape that are not documented in the available experimental data.

After the initial overshoot, the rise velocity settles to a quasi-steady positive value in the two lower Marangoni number cases. In the $Ma = 1723$ case, the drop returns toward the bottom wall after the initial rise, reaches a maximum sink velocity and then appears

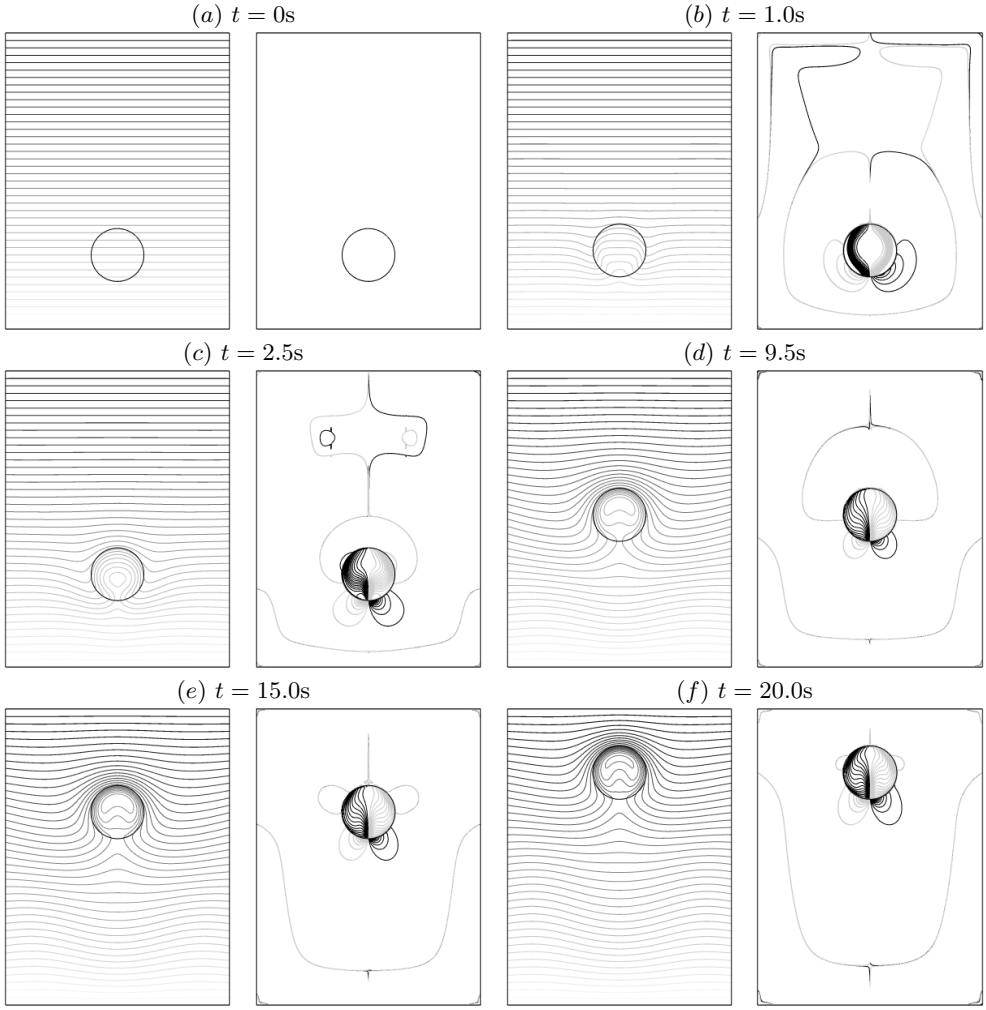

FIGURE 5. Isotherms (left) and vorticity contours (right) for factor 20 higher thermal conductivity case.

to remain stationary near the bottom wall. Comparing the different cases, there is a decrease in the quasi-steady rise velocity with increasing Ma, consistent with transient simulations of non-deformable drops by Yin *et al.* (2008), who only considered $Ma \leq 500$.

Figure 4 also includes a grid convergence study with respect to the peak rise velocity. At $Ma = 86$, first-order convergence is observed. The order is reduced to 0.7 in the $Ma = 345$ case. For $Ma = 1723$ however, the asymptotic regime of convergence has not been reached. This is due to the fact that the thermal boundary layers, which scale as $Ma^{-0.5}$, are not properly resolved on these grids. The results for $Ma = 1723$ are only reported for completeness and should not be considered accurate.

Figures 5 - 7 show snapshots of the isotherms and vorticity contours at 6 different times for the three cases. All three cases show similar vorticity fields, even though the rise velocities are different, indicating that the induced velocity fields in the bulk and drop are similar. In contrast, the isotherms are markedly different. In the $Ma = 86$ case, although

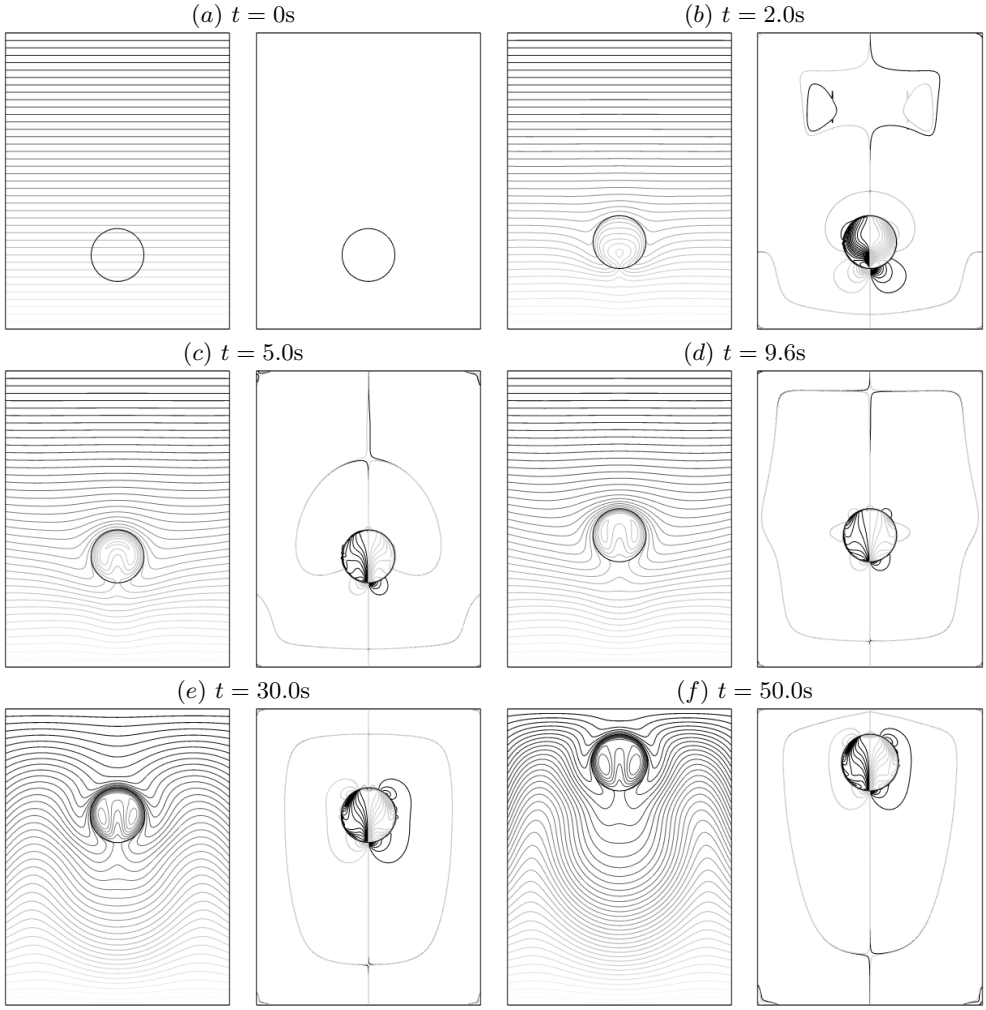

FIGURE 6. Isotherms (left) and vorticity contours (right) for factor 5 higher thermal conductivity case.

the rise velocity of the drop is largest, the temperature field is only slightly disturbed except for the local regions surrounding the drop. In the $Ma = 345$ case, significantly more disturbances to the temperature field can be observed, especially in the wake of the rising drop and even in the regions close to the side walls. In the $Ma = 1723$ case, the isotherms are wrapped around the drop, causing significant inhomogeneities in the bulk. Both higher Marangoni number cases show a significant impact of the experimentally imposed fixed linear temperature gradient up the side walls.

The isotherm inside the drops are benign in the $Ma = 86$ case. This helps maintain a significant temperature gradient at the phase interface, resulting in the relatively high rise velocity. In the large Marangoni number cases, large temperature variations exist inside the drop. The temperature variation along the interface tends to be isothermal, resulting in reduced rise velocities. In the $Ma = 1723$ case, a local temperature inversion can be observed, resulting in a sinking of the drop; it is not clear to what extent this

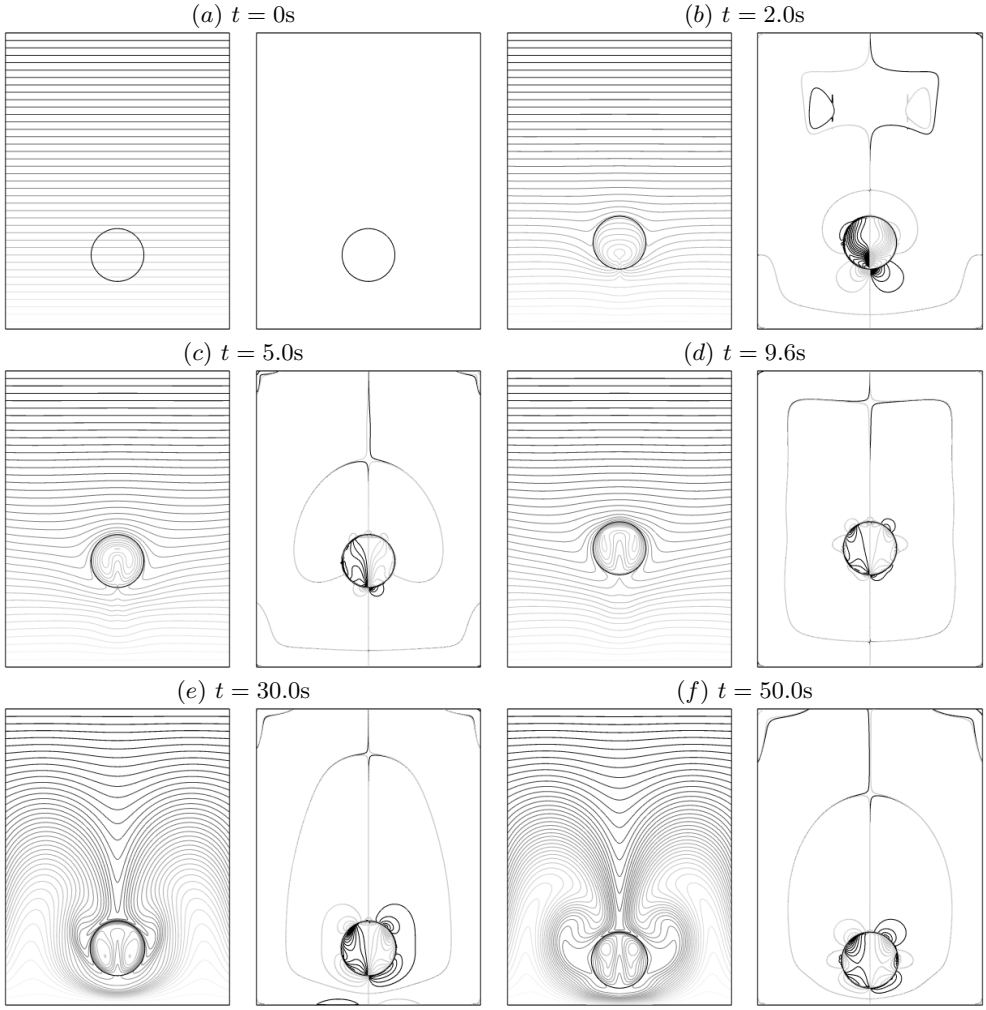

FIGURE 7. Isotherms (left) and vorticity contours (right) for realistic thermal conductivity case.

is due to a lack of numerical resolution. Our results are also influenced by the fact that we compute a planar 2-D problem. In an axisymmetric problem, the dynamics near the pole of the drop may be significantly influenced by the $1/r\partial/\partial r$ terms in the equations. As we noted in Sec. 3.1 for the $Ma \to 0$ test problem, the rise velocity of the planar 2-D drop is about 15% slower than that of a spherical drop.

The observed rise velocity behavior in Fig. 4 can be explained by the isotherm plots. Initially, the drop is subjected to a large temperature gradient at its surface, resulting in strong Marangoni forces and a strong induced flowfield. This results in the initial peak in rise velocity. The strong Marangoni force-induced velocities then lead to a partial (or in the $Ma = 1723$ case, full) homogenization of the temperature at the drop surface, thus reducing the Marangoni force and hence the rise velocity until a quasi-steady state is reached.

4. Conclusion

Predicting surface tension-dominated flows numerically is a challenging task, since numerical errors due to the discretization of this singular term can lead to large errors, so-called spurious currents. In this report, we have presented a numerical method to incorporate surface tension forces both normal and tangential to the phase interface in a consistent manner. The resulting method has been applied to the prediction of the thermocapillary motion of drops. Good agreement with theoretical predictions valid in the limit of zero Marangoni number are obtained.

In the finite Marangoni number case, we have seen that with increasing Ma, the velocity of the drop diminishes. This trend is consistent with experimental observations at large Ma (Treuner *et al.* 1996; Hadland *et al.* 1999; Xie *et al.* 2005), which also report that at large Ma, the drops do not reach a steady velocity and that instead they exhibit complex temporal behavior. Asymptotic and numerical results at large Ma have imposed a steady drop migration velocity (e.g., Ma *et al.* 1999; Balasubramaniam & Subramanian 2000). Our findings indicate that for large Ma, this is not a valid assumption.

At this point, a comment is in order with respect to the characteristic numbers found in atomizing liquid fuel jets with combustion. Assuming temperature differences of order 1500 K on length scales of 1 mm due to flames and liquid drop sizes of $R = 50\,\mu$m, the Reynolds number as defined in this paper is $Re = 120$, the Prandtl number is $Pr = 0.66$, and the Marangoni number is $Ma = 80$. Although the Reynolds number is slightly larger than in the cases analyzed here, the Marangoni number is virtually the same as the lower Ma case in which we were able to obtain grid converged results, pointing to the applicability of the proposed methodology in applications relevant to drop atomization. Note that this does not imply that thermocapillary effects are of importance in atomizing flows with combustion. Only detailed studies of the involved relative time scales and local aerodynamic forces to be performed in the future can answer that question. For this, we have shown that the proposed method is a suitable tool.

REFERENCES

Acrivos, A., Jeffrey, D. J. & Saville, D. A. 1990 Particle migration in suspensions by thermocapillary or electrophoretic motion. *J. Fluid Mech.* **212**, 95–110.

Alonso, J. J., Hahn, S., Ham, F., Herrmann, M., Iaccarino., G., Kalitzin, G., LeGresley, P., Mattsson, K., Medic, G., Moin, P., Pitsch, H., Schluter, J., Svard, M., der Weide, E. V., You, D. & Wu, X. 2006 CHIMPS: A high-performance scalable module for multi-physics simulation. In *42nd AIAA/ASME/SAE/ASEE Joint Propulsion Conference & Exhibit*, *AIAA-Paper* 2006-5274.

Balasubramaniam, R. & Chai, A.-T. 1987 Thermocapillary migration of droplets: an exact solution for small Marangoni numbers. *J. Colloid Interface Sci.* **119**, 531–538.

Balasubramaniam, R. & Subramanian, R. S. 2000 The migration of a drop in a uniform temperature gradient at large Marangoni numbers. *Phys. Fluids* **12**, 733–743.

Borcia, R. & Bestehorn, M. 2007 Phase-field simulations for drops and bubbles. *Phys. Rev. E* **75**, 056309.

Brackbill, J. U., Kothe, D. B. & Zemach, C. 1992 A continuum method for modeling surface tension. *J. Comput. Phys.* **100**, 335–354.

Chen, J. C. & Lee, Y. T. 1992 Effect of surface deformation on thermocapillary bubble migration. *AIAA J.* **30**, 993–998.

Desjardins, O., Blanquart, G., Balarac, G. & Pitsch, H. 2008*a* High order conservative finite difference scheme for variable density low mach number turbulent flows. *J. Comput. Phys.* **227** (15), 7125–7159.

Desjardins, O., Moureau, V. & Pitsch, H. 2008*b* An accurate conservative level set/ghost fluid method for simulating turbulent atomization. *Journal of Computational Physics* **227** (18), 8395–8416.

Hadland, P. H., Balasubramaniam, R., Wozniak, G. & Subramanian, R. S. 1999 Thermocapillary migration of bubbles and drops at moderate to large Marangoni number and moderate Reynolds number in reduced gravity. *Expt. Fluids* **26**, 240–248.

Haj-Hariri, H., Shi, Q. & Borhan, A. 1997 Thermocapillary motion of deformable drops at finite Reynolds and Marangoni numbers. *Phys. Fluids* **9**, 845–855.

Herrmann, M. 2008 A balanced force refined level set grid method for two-phase flows on unstructured flow solver grids. *J. Comput. Phys.* **227** (4), 2674–2706.

Jiang, G.-S. & Peng, D. 2000 Weighted ENO schemes for Hamilton-Jacobi equations. *SIAM J. Sci. Comput.* **21** (6), 2126–2143.

Kang, M., Fedkiw, R. & Liu, X.-D. 2000 A boundary condition capturing method for multiphase incompressible flow. *J. Sci. Comput.* **15** (3), 323–360.

Landau, L. D. & Lifshitz, E. M. 1959 *Fluid Mechanics*. New York: Pergamon.

Levich, V. G. & Krylov, V. S. 1969 Surface-tension-driven phenomena. *Ann. Rev. Fluid Mech.* **1**, 293–316.

Ma, X., Balasubramaniam, R. & Subramanian, R. S. 1999 Numerical simulation of thermocapillary drop motion with internal circulation. *Num. Heat Trans., Part A* **35**, 291–309.

Muradoglu, M. & Tryggvason, G. 2008 A front-tracking method for computation of interfacial flows with soluble surfactants. *J. Comput. Phys.* **227**, 2238–2262.

Nas, S., Muradoglu, M. & Tryggvason, G. 2006 Pattern formation of drops in thermocapillary migration. *Int. J. Heat Mass Transfer* **49**, 2265–2276.

Nas, S. & Tryggvason, G. 2003 Thermocapillary interaction of two bubbles or drops. *Int. J. Multiphase Flow* **29**, 1117–1135.

van der Pijl, S. P., Segal, A. & Vuik, C. 2005 A mass-conserving level-set method for modelling of multi-phase flows. *Int. J. Numer. Meth. Fluids* **47**, 339–361.

Raessi, M., Bussmann, M. & Mostaghimi, J. 2008 A semi-implicit finite volume implementation of the CSF method for treating surface tension in interfacial flows. *Int. J. Numer. Meth. Fluids* (DOI: 10.1002/fld.1857).

Raessi, M., Mostaghimi, J. & Bussmann, M. 2007 Advecting normal vectors: A new method for calculating interface normals and curvatures when modeling two-phase flows. *Journal of Computational Physics* **226** (1), 774–797.

Shu, C. W. 1988 Total-variation-diminishing time discretization. *SIAM J. Sci. Stat. Comput.* **9** (6), 1073–1084.

Someya, S. & Munakata, T. 2005 Measurement of the interface tension of immiscible liquids interface. *J. Crystal Growth* **275**, e343–e348.

Subramanian, R. S. 1992 The motion of bubbles and drops in reduced gravity. In *Transport Processes in Drops, Bubbles, and Particles* (ed. R. D. Chhabra & D. Dekee), pp. 1–41. New York: Hemisphere.

Subramanian, R. S., Balasubramaniam, R. & Wozniak, G. 2002 Fluid mechanics of bubbles and drops. In *Physics of Fluids in Microgravity* (ed. R. Monti), pp. 149–177. London: Taylor and Francis.

Treuner, M., Galindo, V., Gerbeth, G., Langbein, D. & Rath, H. J. 1996 Thermocapillary bubble migration at high Reynolds and Marangoni numbers under low gravity. *J. Colloid Interface Sci.* **179**, 114–127.

Welch, S. W. J. 1998 Transient thermocapillary migration of deformable bubbles. *J. Colloid Interface Sci.* **208**, 500–508.

Wozniak, G., Balasubramaniam, R., Hadland, P. H. & Subramanian, R. S. 2001 Temperature fields in a liquid due to the thermocapillary motion of bubbles and drops. *Expt. Fluids* **31**, 84–89.

Xie, J.-C., Lin, H., Zhang, P., Liu, F. & W.-R., H. 2005 Experimental investigation on thermocapillary drop migration at large Marangoni number in reduced gravity. *J. Colloid Interface Sci.* **285**, 737–743.

Yin, Z., Gao, P., Hu, W. & Chang, L. 2008 Thermocapillary migration of nondeformable drops. *Phys. Fluids* **20**, 082101.

Young, N. O., Goldstein, J. S. & Block, M. J. 1959 The motion of bubbles in a vertical temperature gradient. *J. Fluid Mech.* **6**, 350–356.